Title

Functional Dynamics of the Folded Ankyrin Repeats of IκBα Revealed by Nuclear Magnetic Resonance

Journal

Biochemistry, 48(33)

ISSN

0006-2960

Authors

Cervantes, Carla F
Markwick, Phineus RL
Sue, Shih-Che
et al.

Publication Date

2009-08-25

DOI

10.1021/bi900712r

Peer reviewed

BIOCHEMISTRY
including biophysical chemistry & molecular biology
Article

Biochemistry **2009,** *48,* 8023–8031 8023
DOI: 10.1021/bi900712r

Functional Dynamics of the Folded Ankyrin Repeats of IκBα Revealed by Nuclear Magnetic Resonance†

Carla F. Cervantes,[‖,⊥] Phineus R. L. Markwick,[‡,‖,⊥] Shih-Che Sue,[§] J. Andrew McCammon,[‡,⊥] H. Jane Dyson,*[,§] and Elizabeth A. Komives*[,⊥]

[⊥]*Department of Chemistry and Biochemistry, University of California, San Diego, 9500 Gilman Dr., La Jolla, CA 92093-0378,* [‡]*Howard Hughes Medical Institute and* [§]*Department of Molecular Biology, The Scripps Research Institute, 10550 North Torrey Pines Road, La Jolla, California 92037* [‖]*These authors contributed equally to this work.*

Received April 24, 2009; Revised Manuscript Received July 7, 2009

ABSTRACT: Inhibition of nuclear factor κB (NF-κB) is mainly accomplished by IκBα, which consists of a signal response sequence at the N-terminus, a six-ankyrin repeat domain (ARD) that binds NF-κB, and a C-terminal PEST sequence. Previous studies with the ARD revealed that the fifth and sixth repeats are only partially folded in the absence of NF-κB. Here we report NMR studies of a truncated version of IκBα, containing only the first four ankyrin repeats, IκBα(67−206). This four-repeat segment is well-structured in the free state, enabling full resonance assignments to be made. H−D exchange, backbone dynamics, and residual dipolar coupling (RDC) experiments reveal regions of flexibility. In addition, regions consistent with the presence of micro- to millisecond motions occur periodically throughout the repeat structure. Comparison of the RDCs with the crystal structure gave only moderate agreement, but an ensemble of structures generated by accelerated molecular dynamics gave much better agreement with the measured RDCs. The regions showing flexibility correspond to those implicated in entropic compensation for the loss of flexibility in ankyrin repeats 5 and 6 upon binding to NF-κB. The regions showing micro- to millisecond motions in the free protein are the ends of the β-hairpins that directly interact with NF-κB in the complex.

The ankyrin repeat (AR) is a common motif in proteins that function primarily in protein−protein interactions. The AR is found as a recognition motif in more than 3500 proteins involved in numerous fundamental physiological processes across all kingdoms of life (*1*). For example, ARs form a scaffold for specific, high-affinity interactions involved in the formation of transcription complexes, initiation of immune responses, biogenesis and assembly of cation channels in membranes, regulation of some cell cycle stages, and symbiotic interactions (*2*, *3*). Mutations in genes encoding AR proteins can cause defects in gene expression leading to the onset and progression of disease in animals and humans (*4*). Furthermore, these proteins have recently been successfully targeted in pharmaceutical and biotechnological applications (*5*−*7*).

Most naturally occurring ankyrin repeat domains contain multiple repeats that form a cup-shaped structure in which the helices form the convex surface and the β-hairpins protrude into the concave surface (*1*, *2*, *8*). Each AR consists of 33 amino acids organized into a β-turn/loop−helix−loop−helix fold. The β-hairpin and loop region protrude outward at an angle of ∼90° with respect to the helices, which are arranged in an antiparallel fashion. To date, four structures have been determined by NMR (*9*−*12*) and some 15 more are available from crystallography. Both the convex and concave surfaces of AR domains are used to mediate protein−protein interactions, with the concave surface of the β-hairpins forming the binding interface in the majority of complexes studied so far. Structures of AR domains in complex with their binding partners have also been determined by both NMR (*13*) and crystallography.

The AR domain-containing protein, IκBα, is an inhibitor of transcription factor NF-κB and functions by sequestering NF-κB in the cytoplasm in resting-state cells (*14*). The crystal structure of IκBα in complex with NF-κB (p50/p65) shows that IκBα contacts NF-κB via its six AR domains, forming a discontinuous binding surface in which the first two ARs of IκBα contact the NLS of the p65 subunit of NF-κB and ARs 4−6 contact the dimerization domains of NF-κB p50 and p65 (*15*, *16*). Until recently, there was little structural or dynamic information about free IκBα. The resistance of free IκBα to crystallization (G. Ghosh, personal communication) suggests the presence of conformational disorder in the free protein. ANS binding and H−D exchange experiments monitored by mass spectrometry revealed that free IκBα possesses regions with molten globule character (*17*). H−D exchange experiments further revealed that the ARs of IκBα have different solvent accessibilities, with repeats 1, 5, and 6 being the most solvent accessible (*17*). Urea denaturation experiments demonstrated that the first four repeats of IκBα fold in a cooperative manner, but the fifth and sixth repeats undergo a noncooperative folding transition (*18*). Furthermore, ARs 5 and 6 undergo a coupled folding and binding interaction with NF-κB, whereas the first four repeats exhibit little change in solvent accessibility upon NF-κB binding (*19*).

To understand the architecture and dynamics that hold the well-structured core of free IκBα together, we have undertaken NMR experiments with IκBα(67−206), which comprises the first

†This project was supported by the National Institute of General Medical Sciences (PO1GM071862). C.F.C. acknowledges support from the National Institute of General Medical Sciences (F31GM081897).

*To whom correspondence should be addressed. Phone: (858) 534-3058. Fax: (858) 534-6174. E-mail: ekomives@ucsd.edu.

Published on Web 07/10/2009

FIGURE 1: Sequence alignment between individual repeats of the IκBα AR, with secondary structural elements shown schematically below the sequence. The last line corresponds to the consensus for a stable ankyrin repeat. Residues that correspond to the consensus in each repeat are shown in bold. The IκBα(67−206) fragment is denoted with brackets.

four ARs of the protein (Figure 1). The combined results of NMR dynamics, H−D exchange, and RDC experiments reveal many structural similarities to the crystal structure of NF-κB-bound IκBα, and some surprising differences that were suggested in a previously published all-atom molecular dynamics simulation of IκBα(67−287) (*18*). As suggested by previous H−D exchange mass spectrometry experiments, IκBα(67−206) is well-structured, but backbone ^{15}N order parameters reveal fast time scale dynamics in the variable loops and micro- to millisecond dynamics in the β-hairpins. Furthermore, RDC analysis combined with the results from NMR relaxation and H−D exchange experiments shows that, while the orientations of the eight helices of this domain are very similar to the orientations seen in the crystal structures (*15*, *16*), the outer helix of AR3 is undergoing dynamics which may have implications for the function of IκBα.

MATERIALS AND METHODS

Expression and Purification of IκBα(67−206). IκBα(67−206) in pET11a (Novagen) was transformed into the *Escherichia coli* BL21(DE3) strain. Expression of ^{2}H- and ^{15}N-labeled and ^{2}H-, ^{13}C-, and ^{15}N-labeled IκBα(67−206) was conducted in M9 minimal medium in D_2O supplemented with $^{15}NH_4Cl$ (2 g/L) and [^{13}C]glucose (8 g/L). Cells were acclimated by being grown sequentially in 10 mL cultures of M9ZB, M9, M9(50% D_2O), and M9(90% D_2O). Two 1 L growths were inoculated with the M9(90% D_2O) culture and induced at an OD_{600} of 0.4 with 0.1 mM IPTG for 24 h at 18 °C. The cells were collected by centrifugation at 5000 rpm for 30 min and resuspended in 70 mL/L of culture of 25 mM Tris (pH 7.5), 50 mM NaCl, 0.5 mM EDTA, 10 mM β-mercaptoethanol, 0.3 mM PMSF, and protease inhibitor cocktail (Sigma) and lysed by sonication on ice. The soluble part of the lysate was purified by cation exchange chromatography on a Hi-Load Q-Sepharose 26/10 column (GE Healthcare) using a 1 h gradient from 50 to 500 mM NaCl. The final purification of the protein was conducted on a HiLoad Superdex 75 16/60 gel filtration column (GE Healthcare). The purified protein was concentrated in 4 mL 10K MWCO Amicon concentrators (Millipore) in a fixed angle rotor at 4000 rpm in 15 min intervals to prevent aggregation.

NMR Backbone Resonance Experiments. Backbone resonance assignment experiments with IκBα(67−206) were conducted with 0.5 mM [^{2}H,^{15}N,^{13}C]IκBα(67−206) in 25 mM Tris (pH 7.5), 50 mM NaCl, 50 mM arginine, 50 mM glutamic acid, 5 mM CHAPS, 1 mM EDTA, 1 mM dithiothreitol (DTT), and 2 mM NaN_3 in 90% H_2O and 10% D_2O. Standard HNCA, HN(CO)CA, HNCACB, and HN(COCA)CB experiments were conducted at 20 °C on a Bruker DRX600 instrument (*20*−*22*). The parameters used for these experiments were as follows: HNCA, data size of 2048 (t_3) × 48 (t_2) × 96 (t_1) complex points, with eight scans; HN(CO)CA, data size of 1024 (t_3) × 32 (t_2) × 90 (t_1) complex points, with 16 scans; HN(CA)CB, data size of 1024 (t_3) × 32 (t_2) × 90 (t_1) complex points, with 32 scans; HN-(COCA)CB, data size of 1024 (t_3) × 32 (t_2) × 90 (t_1) complex points, with four scans. The delay time between each scan used was 1.5 s. The data from 36 resonances were assigned but not used in the relaxation and H−D exchange analyses due to overlap (76, 78, 79, 96, 120, 126, 131, 151, 153, 158, 159, 173, 180, and 189−191) or evidence of conformational exchange (69, 70, 72, 73, 81, 82, 85, 89−91, 93, 113, 115, 117, 121, 125, 146−148, 167, and 197). For the comparison of the chemical shifts with random coil values, an additional correction for deuterium isotope effects was also applied (*23*, *24*).

NMR Relaxation Measurements. T_1, T_2, and ^{1}H−^{15}N heteronuclear NOE measurements for 0.5 mM [^{2}H,^{15}N]-IκBα(67−206) were taken at 20 °C on Bruker Avance 501 and DRX600 instruments using standard Bruker programs. T_1 delays were 12 (duplicate), 177, 353, 705, 1057 (duplicate), 1409, 1761, 2201, and 2817 (duplicate) ms. T_2 delays were 9 (duplicate), 13, 17, 21, 29 (duplicate), 37, 53, and 61 (duplicate) ms. ^{1}H−^{15}N NOE saturated and unsaturated spectral measurements were recorded in an interleaved manner. Data were processed using NMRpipe (*25*) and analyzed using NMRView (*26*) and Curvefit (*27*).

H−D Exchange Experiments. The amide H−D exchange was assessed on ^{2}H- and ^{15}N-labeled IκBα(67−206) by rapidly exchanging the protein from H_2O buffer to D_2O buffer (pD 7.1) using a desalting spin column on ice. The sample was immediately put into the NMR tube and into the spectrometer. The progress of the exchange of the amide protons with deuterium was followed by collecting a series of successive ^{1}H−^{15}N HSQC spectra starting immediately after the buffer exchange into D_2O buffer. All exchange experiments were conducted on a Bruker DRX600 instrument at 20 °C, for a total exchange time of 30 h. The first HSQC spectrum was collected after 15 min, and the rest of the spectra were acquired at a 30 min interval for the first 4 h. The last spectrum was acquired with the sample left in the spectrometer overnight (18 h). Protection factors (PF) were determined by calculating k_{int}/k_{ex}, where k_{ex} is the exchange rate constant obtained by fitting a single-exponential function to the intensities of amides in the series of HSQCs and k_{int} is the intrinsic exchange rate constant obtained by using SPHERE (*28*) which corrects for pH and temperature effects. To obtain an estimate for the standard errors, each exchange experiment was repeated twice.

Residual Dipolar Couplings. The isotropic solution consisted of 0.2 mM [^{2}H,^{15}N]IκBα(67−206) in the previously described buffer except without arginine and glutamic acid. The aligned solution was prepared by adding bacteriophage *Pf1* (Asla Biotech) to the [^{15}N]IκBα(67−206) sample. The final sample contained a 9:1 H_2O/D_2O mixture as well as 0.2 mM [^{2}H,^{15}N]IκBα(67−206), 13.5 mg/mL *Pf1* phage, 25 mM Tris-HCl (pH 7.5), 50 mM NaCl, 50 mM arginine, 50 mM glutamic acid, 1 mM EDTA, 2 mM NaN_3, and 2 mM DTT. All spectra for RDC experiments were recorded at 20 °C.

Experiments were conducted using Watergate for water suppression. Residual dipolar couplings were extracted from two-dimensional IPAP ^{1}H−^{15}N HSQC spectra (*29*). Spectra were

processed with NMRpipe (*25*) and analyzed using NMRView (*26*). In total, 102 experimental N−H RDCs were obtained.

Accelerated Molecular Dynamics. The details of the accelerated molecular dynamics (AMD) method have been discussed previously in the literature (*30*, *31*). In AMD, a continuous non-negative bias potential is added to the original potential energy surface. This results in a raising and flattening of the potential energy landscape, decreasing the magnitude of the energy barriers between low-energy states and therefore enhancing the rate of escape from one low-energy conformational state to another while maintaining the essential details of the underlying potential energy surface. The extent to which the potential energy surface is modified depends on the difference between the boost energy and the actual potential. Explicitly, the modified potential, $V^*(r)$, is defined as $V^*(\vec{r}) = V(\vec{r})$ if the potential energy, $V(r)$, is equal to or greater than the boost energy and $V^*(\vec{r}) = V(r) + \Delta V(\vec{r})$ if the potential energy is lower than the boost energy. The energy modification or "bias" is given by

$$\Delta V(\vec{r}) = \frac{[E_b - V(\vec{r})]^2}{\alpha + [E_b - V(\vec{r})]}$$

The extent of acceleration (i.e., how aggressively the conformational space sampling is enhanced) is determined by the choice of the boost energy, E_b, and the acceleration parameter, α. One of the favorable characteristics of AMD is that the corrected canonical ensemble average can be back calculated, so that thermodynamic and other equilibrium properties of the system can be accurately determined.

The protocol employed in this study follows along lines very similar to those of a detailed study of the RDCs in the prototypical system ubiquitin (P. R. L. Markwick et al., manuscript submitted for publication). All simulations were performed using a modified in-house version of the AMBER10 code (*32*). The coordinates for IκBα(67−206) were obtained from the X-ray crystal structure of the IκBα−NF-κB complex (Protein Data Bank entry 1NFI). The system was placed in a periodically repeating box with 8000 water molecules and eight Na^+ counterions. For each simulation, the system was brought to thermodynamic equilibrium at 300 K and 1 bar pressure using a Langevin thermostat with a collision frequency of 3 ps^{-1} and a Berendsen weak-coupling pressure-stat. Simulations were performed for 10 ns each under periodic boundary conditions with a time step of 1 fs. Electrostatic interactions were treated using the particle mesh Ewald method (PME) (*33*) with a direct space sum limit of 10 Å. The ff99SB force field (*34*) was used for the solute residues, and the TIP4P water force field was employed for the solvent molecules. A series of five standard MD simulations acted as a control set, were used as the starting point for the AMD simulations, and also provided an estimate of the average dihedral angle energy (V_{dih}). For IκBα, a "dual boost" AMD methodology (*35*) was used, whereby, in addition to the acceleration that is applied across the torsional terms of the force field, a fixed background acceleration was also applied across the entire potential. This background potential is weak, with the following acceleration parameters: α(tot) = (0.2 × total number of atoms in system in kilocalories per mole) and $E_b(\text{tot}) - V(\text{tot}) = \alpha(\text{tot})$. The AMD simulations were performed for 10 million steps at increasing levels of torsional acceleration with parameters otherwise identical to those of the standard simulations. Twenty AMD simulations were performed at each acceleration level. The corrected canonical ensemble was determined by performing a free energy weighting protocol. The strict Boltzmann reweighting criterion was relaxed, and an initial free energy "prepruning" for each AMD ensemble was performed in which the high-energy structures were stripped out (some 80% of the total trajectory) and the remaining 20% was used to perform the clustering analysis (*36*). To obtain accurate free energy statistics, a reduced set of structures that represent the conformational space sampled in the trajectory were used to seed classical MD simulations. These were then subjected to MM/PBSA analysis which gives the relative free energies. In this way, the AMD simulations were primarily employed to obtain enhanced conformational space sampling, while the free energy statistics are provided by the MM/PBSA analysis. The "optimal" torsional acceleration level for the best reproduction of the experimental RDCs was found to be as follows: $E_b(\text{dih}) - V(\text{dih}) = 600$ kcal/mol and $\alpha(\text{dih}) = 120$ kcal/mol. A detailed description of the results of the entire simulation study will be provided elsewhere (P. R. L. Markwick et al., manuscript submitted for publication).

An SVD analysis was performed to determine the optimal alignment tensor for molecular ensembles generated at each acceleration level (*37*). RDCs calculated from each ensemble at a given acceleration level were then averaged to include the effect of statistical mechanical sampling, as no single free-energy weighted trajectory generated from an AMD simulation reproduced the experimental data as well as the trajectory average. Consistent with our findings for ubiquitin, neither the single X-ray crystal structure nor a set of ensembles generated from standard MD simulations yielded calculated RDCs that fit the experimental data as well as the trajectory-averaged optimal AMD result (P. R. L. Markwick et al., manuscript submitted for publication). Trajectory-averaged order parameters (the orientational distribution of each N−H bond vector) were also determined at the RDC optimal acceleration level.

Residual Dipolar Couplings. We first used PALES and an in-house SVD algorithm to determine the best alignment tensor for the experimental RDC data (using all 102 RDCs and the structure from Protein Data Bank entry 1NFI) (*16*, *38*). The SVD analysis revealed that only 97 of the 102 experimental RDCs could be fit. RDCs for residues 75 and 77, found in the highly flexible N-terminal tail and for residue 81, which had a nonuniform peak shape, were ignored. Two other RDCs, for residues 118 and 184, were removed from the analysis because their values were found to lie significantly outside the alignment tensor window. These five RDCs also did not fit those generated from the X-ray crystal structure and from the MD-generated molecular ensembles. Using the criterion of 1 Hz as the test of significance, the experimental RDCs for three residues (96, 199, and 200) fit better to the crystal structure than to the AMD molecular ensemble. Remarkably, the experimental RDCs for 40 residues showed a significant improvement in the fits to the AMD ensemble as compared to the crystal structure. Of these, 29 (bold) also exhibited long time scale dynamics (residues **77**, **80**, **86**, **87**, **88**, **89**, **98**, **99**, **100**, **101**, **104**, **105**, **106**, 120, 125, 127, 128, 130, **131**, **133**, **135**, **136**, **141**, **144**, **145**, 146, **156**, **158**, **164**, **167**, **168**, 173, 177, **180**, 186, 189, 193, **194**, 201, and **206**). The improvement in the fit of the other 11 RDCs is most likely due to an improved representation of the time- and ensemble-averaged alignment tensor. Slow collective dynamic motions may alter the shape anisotropy of the system, particularly for repeat proteins. The N−H bond vectors associated with these residues happen to lie at a critical angle relative to the alignment tensor, where even small variations in the orientation of the

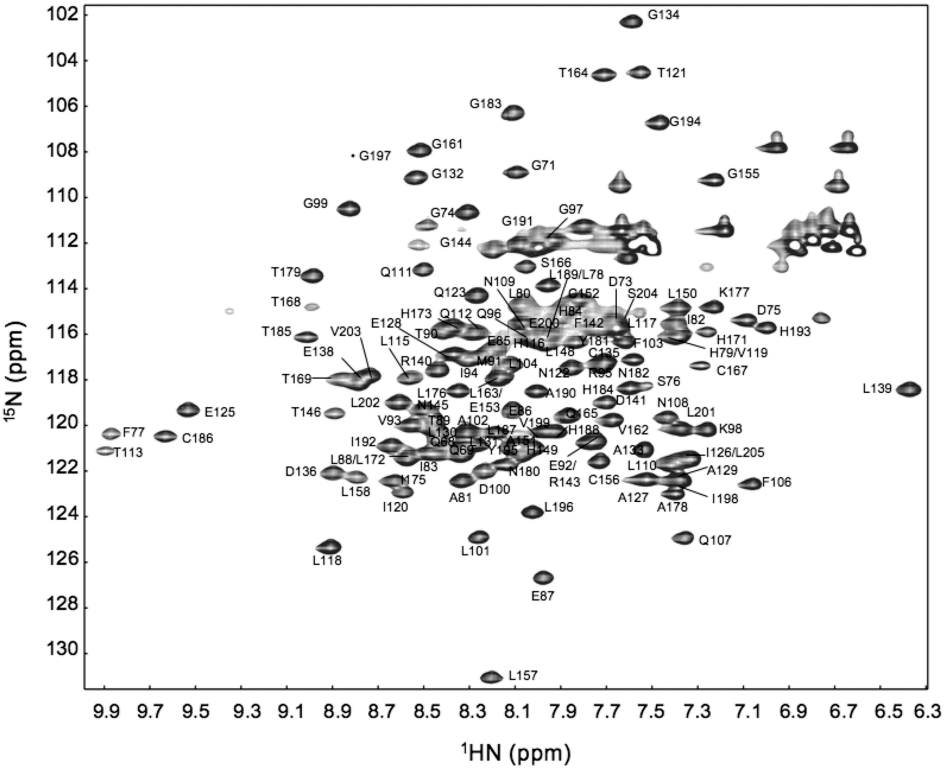

FIGURE 2: 800 MHz ^{1}H−^{15}N TROSY-HSQC spectrum of [^{2}H,^{15}N,^{13}C]IκBα(67−206). The protein concentration was 0.5 mM in 25 mM Tris (pH 7.5), 50 mM NaCl, 50 mM arginine, 50 mM glutamic acid, 5 mM CHAPS, 1 mM EDTA, 1 mM dithiothreitol (DTT), and 2 mM NaN_3 in 90% H_2O and 10% D_2O at 293 K. Assignments for the backbone amides are labeled.

alignment tensor produce substantial changes in the corresponding RDC. A good example of this is residues 120 and 131, which show improvements of 3.37 and 5.14 Hz, respectively.

RESULTS

Backbone Resonance Assignments. IκBα(67−287), which contains all six of the ARs, is marginally stable (*17*), and many of the resonances for the last two ARs are missing (*39*). Truncation of the domain at residue 206 at the end of the fourth repeat resulted in a protein with increased solubility and a much weaker tendency toward aggregation (*18*). The HSQC spectrum of IκBα(67−206) (Figure 2) contained 133 of the 134 expected resonances (all except S159). The resonances were assigned using conventional three-dimensional HNCA, HN(CO)CA, HNCACB, and HN(CO)CACB experiments with ^{2}H-, ^{15}N-, and ^{13}C-labeled protein. The cross-peaks in the HSQC spectrum for IκBα(67−206) were generally of uniform intensity, indicative of a well-structured protein unlike the that seen for IκBα(67−287) (*40*). An exception is residues 69−72 at the N-terminus, which exhibited decreased intensity and broadening, perhaps due to intermediate exchange motions in this part of the protein.

Secondary Structure of IκBα(67−206) in Solution. The chemical shift differences between $^{13}C^{\alpha}$, $^{13}C^{\beta}$, ^{13}CO, ^{15}N, and HN chemical shifts for IκBα(67−206) and the sequence-corrected random coil chemical shift values are shown in Figure 1 of the Supporting Information. The $^{13}C^{\alpha}$ and ^{13}CO secondary chemical shifts showed positive values, and the $^{13}C^{\beta}$ secondary chemical shifts showed the characteristic upfield/near random coil values indicating helical structure. Although the ^{1}HN and ^{15}N chemical shifts are a weaker indicator of secondary structure in general, in IκBα(67−206) these also showed the expected upfield shifts corresponding to the α-helices in the crystal structure (*16*).

Backbone Dynamics of IκBα(67−206). To probe the picosecond to nanosecond scale motions for IκBα(67−206), we measured ^{15}N R_1, ^{15}N R_2, and ^{1}H−^{15}N heteronuclear NOE values at 500 and 600 MHz (Figure 2 of the Supporting Information). The majority of the heteronuclear NOE values were ≥0.8, as expected for a well-structured protein. However, residues 68, 71, and 77 near the N-terminus, residues 99 and 100 in the variable loop between AR1 and AR2, and residue 206 at the C-terminus exhibited values of <0.6, indicative of flexibility on the picosecond to nanosecond time scale.

TENSOR2 was used to analyze the relaxation data (*41*) according to the Model-free formalism (*42*). The resulting order parameters (Figures 3A and 6A) show the presence of picosecond to nanosecond time scale dynamics in the variable loops between each AR and in the β-hairpins at the beginning of each AR. Several regions exhibited longer time scale motions. The β-hairpins fit better to a model that included microsecond to millisecond motions (Figure 3B). Long time scale motions were seen particularly for residues 73, 77, 86, and 88 in AR1, which comprise the majority of the contact surface between the first AR and helix 4 of NF-κB(p65) in the bound complex (*15*, *16*). The latter half of the AR2 β-hairpin (residues 108−113), the entire β-hairpin of AR3 (residues 135−146), and the variable loop between AR3 and AR4 as well as the entire β-hairpin of AR4 (residues 169−185) also showed evidence of longer time scale motions.

Hydrogen−Deuterium Exchange Monitored by NMR Spectroscopy. H−D exchange experiments were performed on IκBα(67−206) to obtain site-specific information about the local stability (and flexibility) of the backbone of IκBα(67−206) toward unfolding processes. Previous mass spectrometry-based H−D exchange experiments (*19*) were performed only for times of up to 5 min, and little amide exchange was observed in this

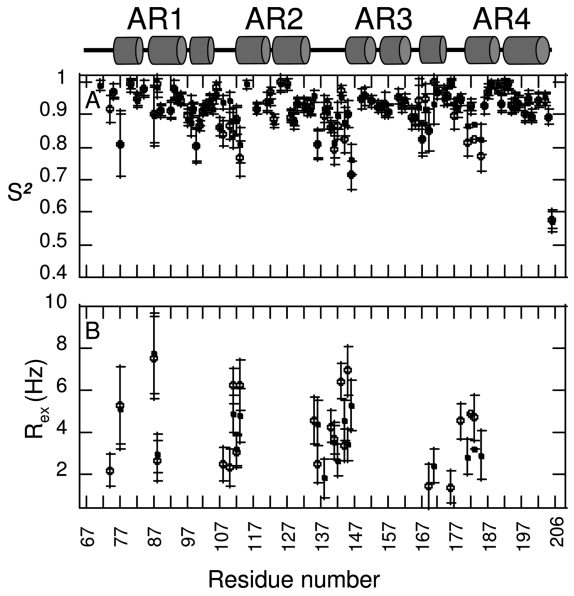

FIGURE 3: Model-free parameters calculated from the ^{15}N relaxation data of free IκBα(67−206) using TENSOR2. (A) Generalized order parameters (S^2) of N−H vectors plotted as a function of residue number. Results from anisotropic and isotropic models were similar. (B) Apparent chemical and conformational exchange contribution (R_{ex}) to the transverse relaxation rate R_2. Residues exhibiting R_{ex} values are located in areas of decreased S^2 values. Results from isotropic (●) and anisotropic (○) fits are shown. Secondary structure elements determined from the crystal structure of the IκBα·NF-κB complex are shown schematically at the top for the sake of comparison.

region of the protein. NMR H−D exchange experiments cannot access such short time scales but do provide information about longer time scales from 20 min to hours. Cross-peak intensities observed in $^1H-^{15}N$ heteronuclear quantum coherence (HSQC) spectra were monitored during a total exchange time of 30 h after rapid solvent exchange into D_2O buffer at pH 7.5 and the data fit to a single-exponential decay for each cross-peak. The protection factors were derived by dividing the intrinsic exchange rate constants for each amino acid (*43*) by the experimentally determined rates. Protection factor values ranged from 10^4 to 10^6, indicative of a very well structured protein (Figure 2D of the Supporting Information). Residues for which the exchange was too rapid for measurement of a protection factor included residues 69, 71, and 74 (N-terminus), 97−103 (AR1/2 variable loop), 132, 134, 140, 142, and 143 (AR 2/3 variable loop), 156, 157, 161, 165, and 166 (AR3 helix 2), 168, 169, 174−177, and 179−185 (AR3/4 variable loop), 187 and 188 (AR4 helix 1), 193−196 (loop between helix 1 and helix 2 in AR4), and 205 and 206 (C-terminus). Higher protection factors were observed in the second AR and the first half of the third AR, consistent with the mass spectrometry-based experiments on shorter time scales for IκBα(67−287) (*19*). The lower protection factors that we observed in the first AR of IκBα(67−206) were also seen in the mass spectrometry-based measurements, but the lower protection factors in the fourth AR are due to the absence of the fifth and sixth ARs from the shorter construct studied here.

Residual Dipolar Couplings in IκBα(67−206). Residual dipolar couplings (RDCs) are determined in partially aligned media and give direct information about the orientation of bond vectors relative to the molecular alignment tensor. RDCs are thus extremely sensitive indicators of the relative orientations of domains or structural elements within a protein (*44*, *45*) and

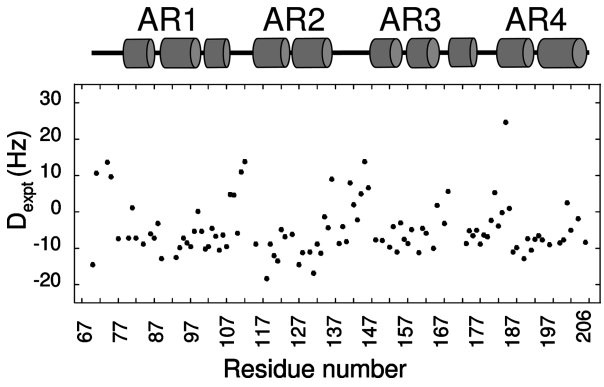

FIGURE 4: Experimentally measured $^1H-^{15}N$ residual dipolar couplings of IκBα(67−206) plotted as a function of residue number. Secondary structure elements determined from the crystal structure of the IκBα·NF-κB complex are shown schematically at the top for the sake of comparison. Helices show consecutive negative RDC values of similar magnitudes, as expected for straight structural arrays, such as α-helices in which N−H bonds are aligned parallel with the helix axis and retain the same orientation with respect to the reference frame. The similar ranges of RDC values for individual helices suggest that the α-helices of free IκBα(67−206) in solution are oriented similarly with respect to the alignment tensor.

can provide a powerful means of characterizing and refining structures, in particular, helical proteins. Helix orientation in crystallographic studies can often be complicated by distortions of the conformation due to crystal packing forces or by crystallization into nonphysiologically relevant configurations (*46*). We pursued RDC measurements to ascertain the relative orientations of the structural elements within IκBα without the need for full-scale NOE measurements (*45*, *47*). To compare the well-structured part of free IκBα in solution to the crystal structure of the IκBα·NF-κB complex, $^1H-^{15}N$ RDCs of [^2H,^{15}N]IκBα(67−206) were measured in an orienting medium containing the filamentous bacteriophage *Pf1*. The measured RDCs showed a periodicity consistent with the repeat structure of the AR domain; all of the helical regions exhibited RDC values between −5 and −10, whereas the variable loops and β-hairpins exhibited large, mainly positive values (Figure 4). The data were analyzed using PALES (*38*) to compare with the crystal structure of IκBα determined in complex with NF-κB published by Harrison and co-workers (*16*): this structure was used because it was better resolved in the region of the first two ARs of IκBα and contained more of the NLS sequence of NF-κB(p65). Figure 5A compares experimentally derived RDC values to those calculated with PALES or using an in-house singular-value decomposition (SVD) algorithm for the crystal structure of NF-κB-bound IκBα. The results showed a surprising amount of scatter, especially considering the high order parameters of the domain. Although RDCs are a structural measure, they reflect dynamic averaging within the structural ensemble up to a time scale of $1/D$ (the inverse of the coupling constant), which is typically several milliseconds (*48*).

Accelerated Molecular Dynamics of IκBα(67−206). Accelerated molecular dynamics (AMD) simulations (see Materials and Methods) were pursued to ascertain whether dynamic processes were contributing to the scatter observed in the RDCs. AMD has been previously employed to successfully interpret RDCs in proteins (*49*). Unrestrained AMD simulations were conducted at increasing acceleration levels to provide systematically enhanced conformational space sampling. Several simulations were obtained for each acceleration level to generate

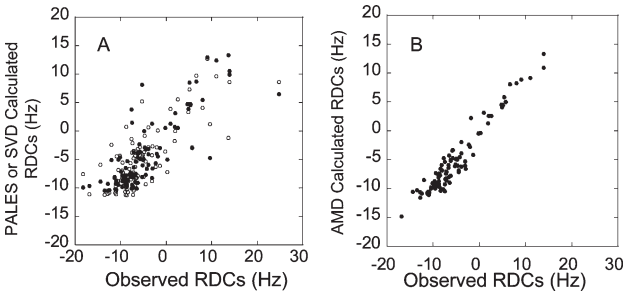

FIGURE 5: (A) Plot of observed vs theoretical residual dipolar couplings measured with PALES for IκBα(67−206) (●) and SVD (○) using the crystal structure of the IκBα·NF-κB complex [Protein Data Bank entry 1IKN (*15*)]. (B) Plot of observed vs AMD-calculated residual dipolar couplings for IκBα(67−206). There is significant improvement in the correlation of the AMD-calculated RDCs with the observed RDCs compared to the results from PALES. For the RDC measurements, an aligned solution was prepared by adding bacteriophage *Pf1* (Asla Biotech) to a [^{15}N]IκBα(67−206) sample. All spectra were acquired at 293 K.

multiple ensembles. SVD analysis of the ensembles collected at each acceleration level was performed to yield the optimal or preferred alignment tensor producing the best possible reproduction of the experimental RDC data for each molecular ensemble. This procedure is identical to that of PALES for obtaining the optimal alignment tensor for the X-ray crystal structure that best reproduces the RDC data, except that it is now being performed on ensembles of structures. It should be emphasized that in comparison to other studies concerning the structural and dynamic interpretation of RDCs, the method presented here is not based on a "fitting" procedure and does not invoke the use of a predefined model of internal dynamics (*50*−*53*). Instead, the RDCs were calculated from the free energy weighted ensembles at increasing acceleration levels. Importantly, the method used here does not require multiple sets of RDC data acquired in different alignment media. The acceleration level that yielded RDCs for the ensembles that best matched those from the experiment was identified (Figure 5B). Clearly, the ensembles represent the measured RDC values much better than the single structure found in the crystal. Of the 98 residues, 75 showed some improvement and 40 RDCs showed a significant improvement of at least 1 Hz. Of these, 29 were associated with residues in regions of the protein that sampled extended conformational space over slower time scales in the optimized AMD ensemble. The other 11 residues that significantly improved were not in regions where slow time scale dynamics were occurring. We attribute the significant improvement in these RDCs to the improved representation of the time-averaged ensemble alignment tensor and recognize that many of these residues had N−H bond vectors that critically depended on this parameter. A representative ensemble of structures from an AMD simulation at the acceleration level that best fit the RDC data is shown in Figure 6B. This ensemble shows structural variations particularly in the outer helices within AR1 and AR3 as well as the variable loops. The trajectory-averaged N−H bond vector order parameters were calculated for the RDC optimal acceleration level and are plotted in Figure 6C. Experimental ^{15}N spin relaxation order parameters, describing dynamics on time scales of up to 6 ns, are also plotted for the sake of comparison. The AMD order parameters calculated at the RDC optimal acceleration level are not limited by the rotation diffusion time but report on dynamic motions up to millisecond time scales ($1/D$, where D is

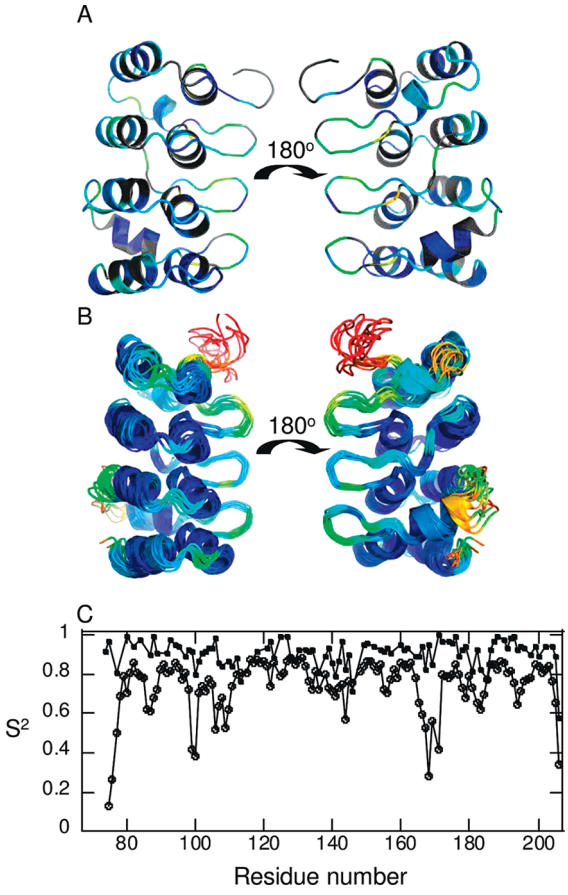

FIGURE 6: (A) Structure of IκBα(67−206) from the IκBα·NF-κB complex [Protein Data Bank entry 1NFI (*16*)] showing the spin relaxation order parameters (S^2) determined from the TENSOR2 analysis of the R_1, R_2, and hNOE data. (B) Ensemble of structures from the AMD simulation using the optimal torsional acceleration level for the best reproduction of the experimental RDCs: E_b(dih) − V(dih) = 600 kcal/mol, and α(dih) = 120 kcal/mol. The calculated order parameters (S^2) determined from the N−H bond vectors from the ensemble-weighted average are shown on the structures. The color scales for panels A and B are from red to blue for S^2 values from 0.1 to 1.0, respectively. (C) Plot of the experimental order parameters (as in Figure 3) (●) compared to those calculated from the optimized AMD simulation (○).

the magnitude of the N−H RDCs). We observe a heterogeneous distribution of long time scale dynamics across the system. Interestingly, many of the regions where the RDC optimal order parameters are lower than those obtained from N−H spin relaxation coincide with those residues that exhibit exchange relaxation (micro- to millisecond dynamics). The experimental spin relaxation (Figure 6A) and the RDC optimal computed (Figure 6B) order parameters are displayed on the structure of IκBα(67−206) using a temperature scale and plotted for the sake of comparison (Figure 6C).

Comparison of Free versus Bound IκBα. We also used TENSOR2 to analyze the R_1, R_2, and heteronuclear NOE data collected previously on NF-κB-bound IκBα(67−287) (*39*) and compared the results to those already presented for IκBα(67−206). Only three residues within the first four ankyrin repeats, 70, 83, and 185, required the model that included R_{ex}, yielding values of 38.6, 9.4, and 16.5 s^{-1}, respectively. Thus, markedly fewer residues showed slow dynamics (R_{ex}) in the complex as compared to the free protein (Figure 3B). The R_{ex} values were determined from the analysis using the anisotropic model in both cases, although similar results were also obtained from the isotropic

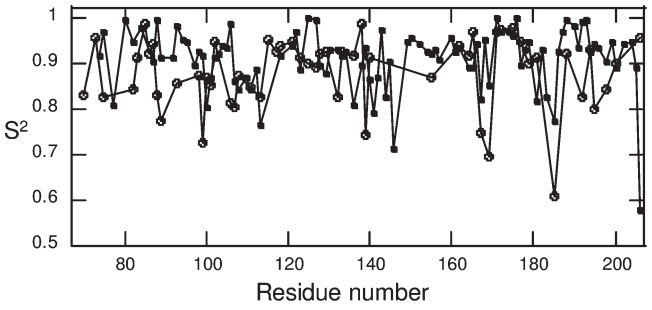

FIGURE 7: Plot of the experimentally determined order parameters (as in Figure 3) for the free protein (●) compared with those for NF-κB-bound IκBα from previously published data (*39*) (○).

model. Order parameters for IκBα bound to NF-κB compared well with those for free IκBα. However, the order parameters in the variable loops were generally lower for IκBα in the complex as compared to free IκBα. This can be explained by the fact that the complex is larger and has a slower rotational diffusion time (13 ns compared to 6 ns); therefore, the order parameters are reporting on internal dynamics over slightly longer time scales (Figure 7). The fact that both isotropic and anisotropic models gave similar results and the fact that the rotational diffusion time is obtained from the R_1/R_2 ratio initially, with no reference to the heteronuclear NOE data, suggest that the effect of the different rotation diffusion times (and models) on the internal dynamics should not be significant.

DISCUSSION

IκBα(67−206) Is a Well-Structured AR Domain. Although many AR domains have been crystallized, the AR domain of IκBα has remained resistant to crystallization except in complex with its binding partner, NF-κB. Earlier work using native-state H−D exchange experiments with short time intervals showed that the fifth and sixth repeats were fully exchanged after only 2 min despite the fact that all of the helical secondary structure seemed to be present (*17*, *18*). Truncation of IκBα at residue 206 resulted in a protein with solubility properties better than those of the full-length AR domain. The NMR results presented here strongly indicate that this fragment of IκBα represents the well-folded part of the IκBα AR domain. The overall high heteronuclear NOE values and amide H−D exchange protection factors obtained for IκBα(67−206) show that this part of the protein behaves as a well-structured AR domain similar to AR proteins which have been structurally and dynamically characterized by NMR, including $p16^{INK4A}$, $p18^{INK4C}$, and $p19^{INK4D}$ (*9*, *54*).

Since the structure of this AR domain was already determined by X-ray crystallography, albeit in complex with its binding partner, NF-κB, we elected not to determine the solution structure of the free protein by standard NOE-based methods but rather to perform RDC experiments to ascertain whether there were any differences between the structures of the AR domain free in solution and bound to NF-κB in the crystal. Careful analysis of the RDC data revealed differences in the outer helices (helix 2) of AR1 and AR3. In addition, it was possible to carry out a full backbone relaxation analysis of AR1−AR4 of IκBα, and the results reveal multiple time scales of motion centered around the binding interface in the complex with NF-κB.

Dynamic Motions in the Outer Helices (helix 2) of AR1 and AR3. We recently reported NMR studies of the full AR domain of IκBα(67−287) bound to NF-κB (*39*). Comparison of the cross-peak intensities of free IκBα(67−206) with those of bound IκBα(67−287) revealed that many of the cross-peaks in AR3 disappeared in the spectrum of the bound form. In addition, protection factors could not be measured for most of AR3 in the complex, but they are high in the free protein (Figure 2 of the Supporting Information). Residues that are missing in the spectra of the IκBα(67−287)·NF-κB complex include residues 135−156, corresponding to the first half of AR3 (*39*). Whereas cross-peaks for residues 147−156 (helix 1) were missing in the bound protein, these are well-ordered, as indicated by high S^2 values, the absence of R_{ex}, and measurable protection factors in free IκBα(67−206) (Figure 3 and Figure 2 of the Supporting Information). Consistent with what was observed in the bound protein, few of the amides in AR3 helix 2 exchanged slowly enough for measurement of protection factors even though the cross-peaks were clearly visible in the HSQC spectrum. These observations were also corroborated by the AMD simulations which showed a broader ensemble of structures for helix 2 of AR3 than for the other helices in the molecule except for helix 2 of AR1, which can be explained by the fact that it is in the first repeat.

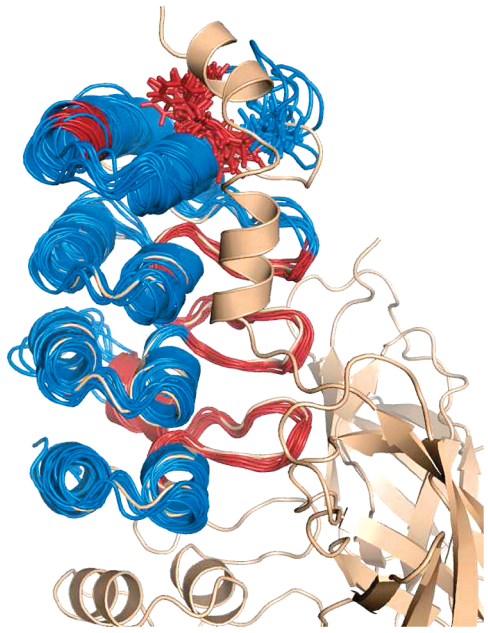

FIGURE 8: Structure of the IκBα·NF-κB complex [Protein Data Bank entry 1NFI (*16*)] showing those residues of IκBα(67−206) with significant R_{ex} colored red.

The observation of slow time scale conformational dynamics in the AR3 outer helix of the free protein is significant for several reasons. First, the interface between the second and third ARs of IκBα is predicted to be the site of folding nucleation, so one might expect that AR3 would not be conformationally mobile (*55*). Second, it is known that the interface between NF-κB and IκBα has two hot spots, one at either end (*56*). This led us to the hypothesis that upon binding, the AR domain of IκBα might be "squeezed". This hypothesis was supported by the observation that cross-peaks in AR3 disappear upon binding, hinting that the squeezing might cause intermediate exchange in AR3. We had previously suggested that the squeezing might contribute to an entropy compensation for folding of the fifth and sixth repeats. However, only small entropy changes are observed upon binding, and prefolding of the fifth and sixth repeats does not result in large entropy "savings" upon binding (*40*). These results suggest

that instead of an overall increase in flexibility of AR3 upon binding, there is a more specific entropy compensation between structural elements within AR3. It is interesting that comparison of the order parameters of residues 67−206 in the free versus bound IκBα actually shows similar and sometimes lower order parameters in the bound form (Figure 7). Overall, the ARD undergoes slower time scale dynamics when free than when bound to NF-κB.

The Binding Interface Has Slow Time Scale Dynamics. Whereas many residues in the free protein exhibited slow time scale dynamics as evidenced by the requirement of additional R_{ex} terms to fit the relaxation data, only three residues exhibited R_{ex} in the bound form. Figure 8 shows the residues for which longer time scale motions were detected mapped onto the structure of the complex (*16*). These residues correspond very well to the surface of the first four ARs of IκBα that contacts NF-κB(p50/p65). The interaction between the ARD of IκBα and NF-κB(p50/p65) involves coupled folding and binding, both the fifth and sixth ARs of IκBα folding onto the dimerization domains of NF-κB (*19*) and of the NLS of p65 folding onto the first AR of IκBα (C. F. Cervantes et al., unpublished data). Comparison of the crystal structures of NF-κB(p50/p65) bound to DNA and bound to IκBα shows that whereas the C-terminal residues of p65, which contain the NLS sequence, are not structured in the DNA-bound complex, they form a bent helical segment when bound to IκBα (*16*, *57*). This latter folding upon binding event results in the interface shown in Figure 8. The NLS folds onto precisely those residues in the well-structured part of IκBα that undergo backbone dynamics on the microsecond to millisecond time scale in the free protein. Such slower motions in one binding partner are thought to be necessary for conformational adjustments that better accommodate the binding partner (*58*). These conformational adjustments may be indicative of "fly-casting" occurring during the binding process (*59*). Fly-casting refers to the observation that a broader conformational ensemble may "capture" the binding partner more readily, thus accelerating the association reaction. Indeed, despite the large and complex interface between NF-κB and IκBα, their association occurs with very rapid kinetics (*60*).

ACKNOWLEDGMENT

We thank Martin Blackledge for useful and interesting discussions.

SUPPORTING INFORMATION AVAILABLE

Additional NMR data, some of which have been published previously as a comparison to data for IκBα in complex with NF-κB. These data include the NMR chemical shift data (Figure 1) and the backbone relaxation data (Figure 2). This material is available free of charge via the Internet at http://pubs.acs.org.

REFERENCES

1. Li, J., Mahajan, A., and Tsai, M. D. (2006) Ankyrin repeat: A unique motif mediating protein-protein interactions. *Biochemistry 45*, 15168–15178.
2. Sedgwick, S. G., and Smerdon, S. J. (1999) The ankyrin repeat: A diversity of interactions on a common structural framework. *Trends Biochem. Sci. 24*, 311–316.
3. Hryniewicz-Jankowska, A., Czogalla, A., Bok, E., and Sikorsk, A. F. (2002) Ankyrins, multifunctional proteins involved in many cellular pathways. *Folia Histochem. Cytobiol. 40*, 239–249.
4. Kumar, A., Takada, Y., Boriek, A. M., and Aggarwal, B. B. (2004) Nuclear factor-κB: Its role in health and disease. *J. Mol. Med. 82*, 434–448.
5. Binz, H. K., Amstutz, P., Kohl, A., Stumpp, M. T., Briand, C., Forrer, P., Grutter, M. G., and Pluckthun, A. (2004) High-affinity binders selected from designed ankyrin repeat protein libraries. *Nat. Biotechnol. 22*, 575–582.
6. Schweizer, A., Roschitzki-Voser, H., Amstutz, P., Briand, C., Gulotti-Georgieva, M., Prenosil, E., Binz, H. K., Capitani, G., Baici, A., Pluckthun, A., and Grutter, M. G. (2007) Inhibition of caspase-2 by a designed ankyrin repeat protein: Specificity, structure, and inhibition mechanism. *Structure 15*, 625–636.
7. Zahnd, C., Wyler, E., Schwenk, J. M., Steiner, D., Lawrence, M. C., McKern, N. M., Pecorari, F., Ward, C. W., Joos, T. O., and Pluckthun, A. (2007) A designed ankyrin repeat protein evolved to picomolar affinity to Her2. *J. Mol. Biol. 369*, 1015–1028.
8. Mosavi, L. K., Cammett, T. J., Desrosiers, D. C., and Peng, Z. Y. (2004) The ankyrin repeat as molecular architecture for protein recognition. *Protein Sci. 13*, 1435–1448.
9. Yuan, C., Li, J., Selby, T. L., Byeon, I. J., and Tsai, M. D. (1999) Tumor suppressor INK4: Comparisons of conformational properties between p16(INK4A) and p18(INK4C). *J. Mol. Biol. 294*, 201–211.
10. Li, J., Byeon, I. J., Ericson, K., Poi, M. J., O'Maille, P., Selby, T., and Tsai, M. D. (1999) Tumor suppressor INK4: Determination of the solution structure of p18INK4C and demonstration of the functional significance of loops in p18INK4C and p16INK4A. *Biochemistry 38*, 2930–2940.
11. Luh, F. Y., Archer, S. J., Domaille, P. J., Smith, B. O., Owen, D., Brotherton, D. H., Raine, A. R., Xu, X., Brizuela, L., Brenner, S. L., and Laue, E. D. (1997) Structure of the cyclin-dependent kinase inhibitor p19Ink4d. *Nature 389*, 999–1003.
12. Yang, Y., Nanduri, S., Sen, S., and Qin, J. (1998) The structural basis of ankyrin-like repeat function as revealed by the solution structure of myotrophin. *Structure 6*, 619–626.
13. Yang, Y., Wang, X., Hawkins, C. A., Chen, K., Vaynberg, J., Mao, X., Tu, Y., Zuo, X., Wang, J., Wang, Y. X., Wu, C., Tjandra, N., and Qin, J. (2009) Structural Basis of Focal Adhesion Localization of LIM-only Adaptor PINCH by Integrin-linked Kinase. *J. Biol. Chem. 284*, 5836–5844.
14. Baeuerle, P. A., and Baltimore, D. (1998) IκB: A specific inhibitor of the NF-κB transcription factor. *Science 242*, 540–546.
15. Huxford, T., Huang, D. B., Malek, S., and Ghosh, G. (1998) The crystal structure of the IκBα/NF-κB complex reveals mechanisms of NF-κB inactivation. *Cell 95*, 759–770.
16. Jacobs, M. D., and Harrison, S. C. (1998) Structure of an IκBα/NF-κB complex. *Cell 95*, 749–758.
17. Croy, C. H., Bergqvist, S., Huxford, T., Ghosh, G., and Komives, E. A. (2004) Biophysical characterization of the free IκBα ankyrin repeat domain in solution. *Protein Sci. 13*, 1767–1777.
18. Ferreiro, D. U., Cervantes, C. F., Truhlar, S. M., Cho, S. S., Wolynes, P. G., and Komives, E. A. (2007) Stabilizing IκBα by "consensus" design. *J. Mol. Biol. 365*, 1201–1216.
19. Truhlar, S. M., Torpey, J. W., and Komives, E. A. (2006) Regions of IκBα that are critical for its inhibition of NF-κB.DNA interaction fold upon binding to NF-κB. *Proc. Natl. Acad. Sci. U.S.A. 103*, 18951–18956.
20. Grzesiek, S., and Bax, A. (1992) Improved 3D triple-resonance NMR techniques applied to a 31 kDa protein. *J. Magn. Reson. 96*, 432–440.
21. Wittekind, M., and Mueller, L. (1993) HNCACB, a high-sensitivity 3D NMR experiment to correlate amide-proton and nitrogen resonances with the α- and β-carbon resonances in proteins. *J. Magn. Reson. 101*, 201–205.
22. Yamazaki, T., Lee, W., Arrowsmith, C. H., Muhandiram, D. R., and Kay, L. E. (1994) A suite of triple-resonance NMR experiments for the backbone assignmnet of ^{15}N, ^{13}C, ^{2}H labeled proteins with high sensitivity. *J. Am. Chem. Soc. 116*, 11655–11666.
23. Gardner, K. H., Rosen, M. K., and Kay, L. E. (1997) Global folds of highly deuterated, methyl-protonated proteins by multidimensional NMR. *Biochemistry 36*, 1389–1401.
24. Schwarzinger, S., Kroon, G. J., Foss, T. R., Chung, J., Wright, P. E., and Dyson, H. J. (2001) Sequence-dependent correction of random coil NMR chemical shifts. *J. Am. Chem. Soc. 123*, 2970–2978.
25. Delaglio, F., Grzesiek, S., Vuister, G. W., Zhu, G., Pfeifer, J., and Bax, A. (1995) NMRPipe: A multidimensional spectral processing system based on UNIX pipes. *J. Biomol. NMR 6*, 277–293.
26. Johnson, B. A. (2004) Using NMRView to visualize and analyze the NMR spectra of macromolecules. *Methods Mol. Biol. 278*, 313–352.
27. Mandel, A. M., Akke, M., and Palmer, A. G.III (1995) Backbone dynamics of *Escherichia coli* ribonuclease HI: Correlations with structure and function in an active enzyme. *J. Mol. Biol. 246*, 144–163.

28. Bai, Y., Milne, J. S., Mayne, L., and Englander, S. W. (1993) Primary structure effects on peptide group hydrogen exchange. *Proteins 17*, 75–86.
29. Ottiger, M., Delaglio, F., and Bax, A. (1998) Measurement of J and dipolar couplings from simplified two-dimensional NMR spectra. *J. Magn. Reson. 131*, 373–378.
30. Hamelberg, D., Mongan, J., and McCammon, J. A. (2004) Accelerated molecular dynamics: A promising and efficient simulation method for biomolecules. *J. Chem. Phys. 120*, 11919–11929.
31. Hamelberg, D., and McCammon, J. A. (2005) Fast peptidyl cis-trans isomerization within the flexible Gly-rich flaps of HIV-1 protease. *J. Am. Chem. Soc. 127*, 13778–13779.
32. Case, D. A., Darden, T. A., Cheatham, T. E. I., Simmerling, C. L., Wang, J., Duke, R. E., Luo, R., Crowley, M., Ross, W. C., Zhang, W., Merz, K. M., Wang, B., Hayik, S., Roitberg, A., Seabra, G., Kolossváry, I., Wong, K. F., Paesani, F., Vanicek, J., Wu, X., Brozell, S. R., Steinbrecher, T., Gohlke, H., Yang, L., Tan, C., Mongan, J., Hornak, V., Cui, G., Mathews, D. H., Seetin, M. G., Sagui, C., Babin, V., and Kollman, P. A. (2008) AMBER 10 , University of California, San Francisco.
33. Cheatham, T. E. I., Miller, J. L., Fox, T., Darden, T. A., and Kollman, P. A. (1995) Molecular Dynamics Simulations on Solvated Biomolecular Systems: The Particle Mesh Ewald Method Leads to Stable Trajectories of DNA, RNA, and Proteins. *J. Am. Chem. Soc. 117*, 4193–4194.
34. Hornak, V., Abel, R., Okur, A., Strockbine, B., Roitberg, A., and Simmerling, C. (2006) Comparison of multiple Amber force fields and development of improved protein backbone parameters. *Proteins 65*, 712–725.
35. Hamelberg, D., de Oliveira, C. A., and McCammon, J. A. (2007) Sampling of slow diffusive conformational transitions with accelerated molecular dynamics. *J. Chem. Phys. 127*, 155102.
36. Massova, I., and Kollman, P. A. (1999) Computational Alanine Scanning To Probe Protein-Protein Interactions: A Novel Approach To Evaluate Binding Free Energies. *J. Am. Chem. Soc. 121*, 8133–8143.
37. Showalter, S. A., and Bruschweiler, R. (2007) Quantitative molecular ensemble interpretation of NMR dipolar couplings without restraints. *J. Am. Chem. Soc. 129*, 4158–4159.
38. Zweckstetter, M. (2008) NMR: Prediction of molecular alignment from structure using the PALES software. *Nat. Protoc. 3*, 679–690.
39. Sue, S. C., Cervantes, C., Komives, E. A., and Dyson, H. J. (2008) Transfer of Flexibility between Ankyrin Repeats in IκBα upon Formation of the NF-κB Complex. *J. Mol. Biol. 380*, 917–931.
40. Truhlar, S. M. E., Mathes, E., Cervantes, C. F., Ghosh, G., and Komives, E. A. (2008) Pre-folding IκBα alters control of NF-κB signaling. *J. Mol. Biol. 380*, 67–82.
41. Dosset, P., Hus, J. C., Marion, D., and Blackledge, M. (2001) A novel interactive tool for rigid-body modeling of multi-domain macromolecules using residual dipolar couplings. *J. Biomol. NMR 20*, 223–231.
42. Lipari, G., and Szabo, A. (1981) Nuclear magnetic resonance relaxation in nucleic acid fragments: Models for internal motion. *Biochemistry 20*, 6250–6256.
43. Englander, S. W., Mayne, L., Bai, Y., and Sosnick, T. R. (1997) Hydrogen exchange: The modern legacy of Linderstrom-Lang. *Protein Sci. 6*, 1101–1109.
44. Bax, A., Kontaxis, G., and Tjandra, N. (2001) Dipolar couplings in macromolecular structure determination. *Methods Enzymol. 339*, 127–174.
45. Prestegard, J. H., Bougault, C. M., and Kishore, A. I. (2004) Residual dipolar couplings in structure determination of biomolecules. *Chem. Rev. 104*, 3519–3540.
46. Tolman, J. R., and Ruan, K. (2006) NMR residual dipolar couplings as probes of biomolecular dynamics. *Chem. Rev. 106*, 1720–1736.
47. Tolman, J. R., Al-Hashimi, H. M., Kay, L. E., and Prestegard, J. H. (2001) Structural and dynamic analysis of residual dipolar coupling data for proteins. *J. Am. Chem. Soc. 123*, 1416–1424.
48. Tolman, J. R., Flanagan, J. M., Kennedy, M. A., and Prestegard, J. H. (1997) NMR evidence for slow collective motions in cyanometmyoglobin. *Nat. Struct. Biol. 4*, 292–297.
49. Markwick, P. R. L., Bouvignies, G., and Blackledge, M. (2007) Exploring multiple time-scale motions in protein GB3 using accelerated molecular dynamics and NMR spectroscopy. *J. Am. Chem. Soc. 129*, 4724–4730.
50. Tolman, J. R. (2002) A novel approach to the retrieval of structural and dynamic information from residual dipolar couplings using several oriented media in biomolecular NMR spectroscopy. *J. Am. Chem. Soc. 124*, 12020–12030.
51. Meiler, J., Peti, W., and Griesinger, C. (2003) Dipolar Couplings in Multiple Alignments Suggest α Helical Motion in Ubiquitin. *J. Am. Chem. Soc. 125*, 8072–8073.
52. Bouvignies, G., Markwick, P., Bruschweiler, R., and Blackledge, M. (2006) Simultaneous determination of protein backbone structure and dynamics from residual dipolar couplings. *J. Am. Chem. Soc. 128*, 15100–15101.
53. Lange, O. F., Lakomek, N. A., Farès, C., Schröder, G. F., Walter, K. F., Becker, S., Meiler, J., Grubmuller, H., Griesinger, C., and de Groot, B. L. (2008) Recognition dynamics up to microseconds revealed from an RDC-derived ubiquitin ensemble in solution. *Science 320*, 1471–1475.
54. Renner, C., Baumgartner, R., Noegel, A. A., and Holak, T. A. (1998) Backbone dynamics of the CDK inhibitor p19(INK4d) studied by ^{15}N NMR relaxation experiments at two field strengths. *J. Mol. Biol. 283*, 221–229.
55. Ferreiro, D. U., Cho, S. S., Komives, E. A., and Wolynes, P. G. (2005) The energy landscape of modular repeat proteins: Topology determines folding mechanism in the ankyrin family. *J. Mol. Biol. 354*, 679–692.
56. Bergqvist, S., Ghosh, G., and Komives, E. A. (2008) The IκBα/NF-κB complex has two hot-spots, one at either end of the interface. *Protein Sci. 17*, 2051–2058.
57. Chen, F. E., Huang, D. B., Chen, Y. Q., and Ghosh, G. (1998) Crystal structure of p50/p65 heterodimer of transcription factor NF-κB bound to DNA. *Nature 391*, 410–413.
58. Bonvin, A. M., Boelens, R., and Kaptein, R. (2005) NMR analysis of protein interactions. *Curr. Opin. Chem. Biol. 9*, 501–508.
59. Shoemaker, B. A., Portman, J. J., and Wolynes, P. G. (2000) Speeding molecular recognition by using the folding funnel: The fly-casting mechanism. *Proc. Natl. Acad. Sci. U.S.A. 97*, 8868–8873.
60. Bergqvist, S., Croy, C. H., Kjaergaard, M., Huxford, T., Ghosh, G., and Komives, E. A. (2006) Thermodynamics reveal that helix four in the NLS of NF-κB p65 anchors IκBα, forming a very stable complex. *J. Mol. Biol. 360*, 421–434.